Soft Matter

PAPER

View Article Online
View Journal | View Issue

Cite this: *Soft Matter*, 2022, **18**, 1991

Electric field induced macroscopic cellular phase of nanoparticles†

Abigail Rendos, ‡[a] Wenhan Cao, ‡§[b] Margaret Chern, [a] Marco Lauricella, [c] Sauro Succi, [d] Jörg G. Werner, [ab] Allison M. Dennis [ae] and Keith A. Brown *[abf]

Received 19th November 2021,
Accepted 20th January 2022

DOI: 10.1039/d1sm01650d

rsc.li/soft-matter-journal

A suspension of nanoparticles with very low volume fraction is found to assemble into a macroscopic cellular phase that is composed of particle-rich walls and particle-free voids under the collective influence of AC and DC voltages. Systematic study of this phase transition shows that it was the result of electrophoretic assembly into a two-dimensional configuration followed by spinodal decomposition into particle-rich walls and particle-poor cells mediated principally by electrohydrodynamic flow. This mechanistic understanding reveals two characteristics needed for a cellular phase to form, namely (1) a system that is considered two dimensional and (2) short-range attractive, long-range repulsive interparticle interactions. In addition to determining the mechanism underpinning the formation of the cellular phase, this work presents a method to reversibly assemble microscale continuous structures out of nanoscale particles in a manner that may enable the creation of materials that impact diverse fields including energy storage and filtration.

Introduction

Electric fields provide a flexible means to manipulate soft matter, however, they interact with materials in electrolytic solutions through numerous distinct phenomena making the outcome of field-directed assembly difficult to predict. When a suspension of polarizable particles experiences a spatially uniform electric field, their induced dipoles lead them to form isolated chains along field lines, causing solidification through the electrorheological effect.[1–3] The materials formed during the electrorheological effect are not continuous in that individual chains or columns are not connected to their neighbours. In contrast, suspensions have also been experimentally observed to assemble into macroscopic porous structures with particle-rich walls and particle-poor voids,[4–8] even though this phase has not been completely recapitulated in simulation.[3,9–11] Interestingly, these cellular phase structures do form continuous materials in that the walls form a two-dimensional network that extends across the entire region. Further, the size of the pores – both the voids formed by the cells and the space between particles in the particle-rich walls – can be controlled, indicating that these cellular phases have the potential to become hierarchically-structured mesoporous materials. While these porous structures suggest a path to realizing continuous mesoporous solids with extremely low densities, the origin of this phase is not clear even though, and perhaps because, the cellular phase was observed in vastly different systems spanning orders of magnitude in particle size, particle volume fraction, and electric excitation. While electrohydrodynamic (EHD) flow was identified as the primary mechanism of formation in two instances[4,5] and electroosmotic (EO) flow in another,[8] the other two examples list the interactions between induced dipoles as the origin of the structure.[6,7] Overall, the lack of a cohesive and encompassing explanation for the formation of the cellular phase hinders the ability to design macroscopic porous structures.

Here, we find that a nanoparticle suspension exhibits a macroscopic cellular phase when an AC voltage V_{AC} and DC voltage V_{DC} are simultaneously applied, despite using quantum dot (QD) particles with a diameter and volume fraction both at least an order of magnitude smaller than all prior examples of the cellular phase. Indeed, systematic study revealed that the cellular phase only formed in the presence of both V_{DC} and V_{AC} at volume fraction-dependent critical voltages. The complex interactions required to produce a cellular phase in this system include (1) electrochemistry to generate a DC current, (2) electrophoresis to aggregate particles into a 2D arrangement on one

[a] *Division of Materials Science & Engineering, Boston University, Boston, MA, USA. E-mail: brownka@bu.edu*
[b] *Department of Mechanical Engineering, Boston University, Boston, MA, USA*
[c] *Istituto per le Applicazioni del Calcolo, Consiglio Nazionale delle Ricerche, via dei Taurini 19, Rome, 00185, Italy*
[d] *Center for Life Nano-Neuro Science at La Sapienza, Rome, Italy*
[e] *Biomedical Engineering Department, Boston University, Boston, MA, USA*
[f] *Physics Department, Boston University, Boston, MA, USA*

† Electronic supplementary information (ESI) available. See DOI: 10.1039/d1sm01650d

‡ Contributed equally.

§ Present address: School of Information Science and Technology, ShanghaiTech University, Shanghai, 201210, China.

electrode, and (3) an instability driven by the long-ranged repulsive and short-ranged attractive EHD flow that nucleates at regions on the electrode with high local field enhancement. Notably, EO and other purely attractive interactions are competitive with the cellular phase and instead drive the system towards a cluster-phase (*i.e.* pearl chaining). This mechanistic explanation was compared to all previous examples of the electrically-mediated cellular phase to identify a set of unifying factors that appear to always be present, namely that the system adopts an effective 2D arrangement and features an in-plane interaction that is short-range attractive and long-range repulsive. This understanding paves the way towards the concerted formation of hierarchical porous structures that may impact fields including energy storage and filtration.[12,13]

Experimental methods

As a model system for assembly, poly(maleic anhydride-*alt*-1-octadecene) (PMAO)-coated CdSe/CdS quantum dots (QDs),[14,15] were suspended in dilute borate buffer (3.125 mM, 5.5 nm Debye screening length)[16] at a volume fraction $\varphi = 6 \times 10^{-5}$ which is equivalent to a 25 nM particle concentration. For a typical assembly experiment, indium tin oxide (ITO) slides (2277 – University Wafer, 703176 – Sigma Aldrich) were prepared by sonicating them in acetone and subsequently isopropanol for 5 min each before drying them under an N_2 stream. Finally, the ITO slides were placed into the 3D printed frame pictured in Fig. S2(a) (ESI†). A laser-cut polyimide spacer (2271K72 – McMaster) with a thickness fixed by a 177 ± 1 μm was then placed onto one of the ITO slides and 4 μL of the suspension was pipetted onto the ITO-coated glass and covered with a second ITO-coated glass slide to form a fluid cell as shown in Fig. 1(a).

This complete cell was then transferred to an Olympus BX43 microscope with a GS3-U3-120S6M-C Grasshopper camera. A filter cube with an emission wavelength at 642 nm, 75 nm BW (67-036 – Edmund Optics Inc.), a short-pass excitation filter with a cutoff at 500 nm (84-706 – Edmund Optics Inc.), and a dichroic with cutoff at 550 nm (DMLP550R – ThorLabs Inc.) were used to visualize the photoluminescent QDs. Alligator-clip leads were attached to a corner of each ITO-coated slide as shown in Fig. S2(b) (ESI†) in order to apply an AC voltage with amplitude V_{AC} and DC offset voltage V_{DC} across the fluid cell using a Keysight 33521B waveform generator. Fluorescence micrographs were taken using 5× magnification with a 500 ms exposure time and 14 dB gain to have sufficient contrast. In most experiments, such as those conducted in Fig. 1 and 5 along with ESI† Fig. S3, S4, and S7, V_{AC} = 2 V with frequency f = 500 kHz and V_{DC} = 2.2 V.

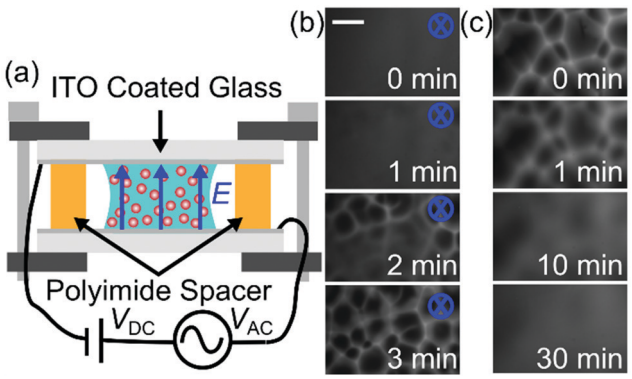

Fig. 1 (a) Fluid cell consisting of two ITO-coated glass slides separated by a polyimide spacer and containing a suspension of quantum dots (QDs). DC and AC voltages, V_{DC} and V_{AC} respectively, were applied across the fluid cell. (b) Fluorescent micrographs showing the formation of the cellular phase when V_{DC} = 2.2 V and V_{AC} = 2 V were applied to a suspension with volume fraction $\varphi = 6 \times 10^{-5}$. The scale bar depicts 500 μm. (c) Fluorescent micrographs showing that after V_{DC} and V_{AC} were turned off, the particles diffused back into a homogenous distribution.

Results and discussion

Simultaneously applying V_{AC} and V_{DC} across the QD suspension resulted in a cellular phase at strikingly low φ, particle size, and field intensities. Specifically, setting V_{DC} = 2.2 V and V_{AC} = 2 V amplitude at 500 kHz, the particles assembled into a cellular phase over the course of a few minutes as shown in Fig. 1(b). To determine whether this process was reversible, the field was subsequently switched off, which led the suspension to gradually homogenize through diffusion, as seen in Fig. 1(c). Additionally, the formation of the cellular phase was reversible over multiple cycles as can be seen in Fig. S3 (ESI†) which shows the same fluid cell exhibiting the cellular phase for six on/off cycles. Given that this phase has not been previously observed for particles with hydrodynamic diameters <100 nm, we considered whether this could be specific to these QDs. Thus, we repeated this experiment with two different sizes of commercially available fluorophore-doped polystyrene nanoparticles and again observed the cellular phase (Fig. S4, ESI†), showing that this phase is not restricted to these QDs, or one particular particle size.

To explore the mechanism of the cellular phase and whether it originated from forces between induced dipoles, we compute the non-dimensional parameter $\Lambda = \frac{\alpha V^2}{8 k_B T H^2}$, which reflects the importance of induced dipole interactions between particles relative to thermal energy given particle polarizability a, applied voltage V, electrode separation H, Boltzmann's constant k_B, and temperature T. Here, we estimate $\Lambda \sim 0.008$, indicating that induced dipole mediated assembly should not occur and that other interactions must drive the formation of the cellular phase. Another potential mechanism is suggested by the resemblance of the cellular phase to Benárd cells where gravity-driven natural convection from density gradients produces similar cells.[17–19] Thus, we repeated the experimental conditions shown in Fig. 1 with the cell rotated 90° such that gravity pointed along the electrodes and the same cellular structure formed (Fig. S5, ESI†), indicating that natural convection is not responsible for the cellular phase.

In order to explore the mechanism of the cellular phase, we examined the contributions of V_{DC} and V_{AC}. Specifically, we performed a series of experiments holding V_{AC} fixed while V_{DC} was incrementally increased from 0 to 2.6 V in steps of 0.2 V. A fluorescence micrograph was taken at each increment after equilibrating for 4 min. The observed gradual transition from a uniform suspension to an ordered cellular phase was apparent and shown in Fig. 2(a). To analyze these experiments, the fluorescent pattern in each image was manually classified as having (1) a uniform background (no phase) (2) an interconnected series of lines (cellular phase), (3) a series of isolated bright spots (cluster phase) or (4) indeterminate (transition phase). These classifications are shown in Fig. 2(b), which clearly shows that a minimum V_{DC} of $\sim$1.8 V was required to form the cellular phase. The full series of images are shown in Fig. S6 (ESI†).

While V_{DC} was required to form the cellular phase, the origin of the $\sim$1.8 V threshold voltage, or the dominant physical effect of V_{DC}, was not clear. The relevance of the DC field is especially noteworthy when one considers that electrolyte ions will accumulate on oppositely charged electrodes, giving rise to an electrode polarization that screens the DC field, thus preventing a strong DC component in the bulk.[20,21] One process that could maintain a steady-state DC field is a constant flow of ions across the chamber mediated by their electrochemical generation/annihilation at the anode and cathode. Electrochemical reactions at the electrodes could also explain the V_{DC} threshold as highly non-linear currents are common in electrochemistry due to reaction-specific standard reduction/oxidation potentials and mass transport effects.[22] To determine whether electrochemical currents were present, two-electrode cyclic voltammetry measurements were conducted on the cell, confirming that electrochemical reactions were present and resulted in an appreciable current when $V_{DC} > 1.5$ V (Fig. S7, ESI†). The observed reactions were likely due to a combination of water electrolysis and ITO degradation.[23,24] While the current turn-on behavior was commensurate with the onset of the cellular phase, we sought to establish a more definitive link between electrochemical reactions on the electrodes and the cellular phase. Thus, we coated the surface of the ITO electrodes with an insulating layer of poly(methyl methacrylate) (PMMA) to prevent electrochemical reactions from occurring and repeated the assembly experiment. After this treatment, the cellular phase did not form at any voltage (Fig. S8, ESI†), verifying that electrochemistry was required for the cellular phase to form.

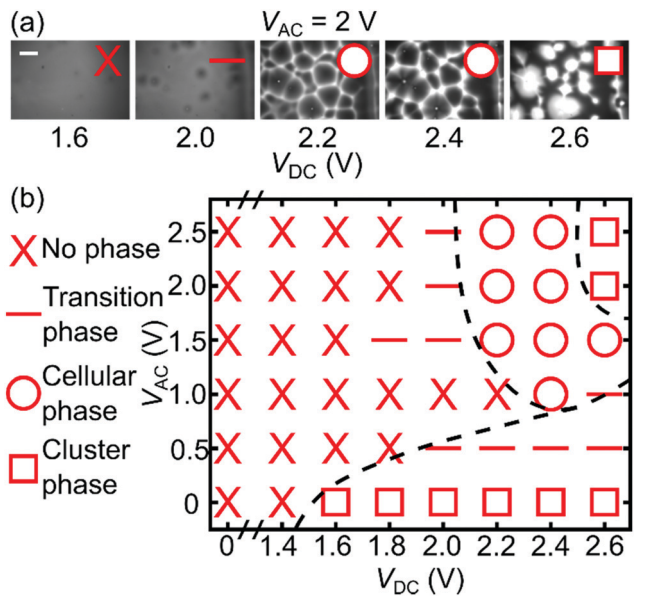

Fig. 2 (a) Phase transitions as V_{DC} was increased with V_{AC} = 2.0 V for $\varphi = 6 \times 10^{-5}$. The scale bar depicts 500 μm. (b) Phase diagram depicting transition from no phase to either cellular or cluster phases. Ambiguous images were classified as transition. Full data is shown in Fig. S6 (ESI†).

Due to the electrochemical reactions at the electrodes, a steady-state DC field persisted in the chamber and led to electrophoresis of the QDs and a subsequent increase in their local concentration on one electrode. Since these QDs had a slightly negative zeta potential,[25] they will accumulate on the positively charged electrode and form a thin particle-dense film, calculated to be about a monolayer in thickness. In order to determine whether the particles were electrophoretically active, we conducted an experiment with electrodes spaced 1.4 mm apart and imaged the behavior at V_{DC} = 4 V from the side of the cell which confirmed the expected movement of the particle to the positive electrode (Fig. S9, ESI†). To understand the fate of this initially uniform film, it is useful to consider that the magnitude of V_{AC} determines whether it will adopt a cellular or cluster phase, as shown in Fig. 2(b). Particles on a substrate will interact through two types of electrically-induced fluid flows: EO flow and EHD flow.[22,26,27] While EO flow is a DC phenomenon, EHD flows arise from both V_{AC} and V_{DC}.[22,26] Interestingly, these effects are expected to produce contrasting flow fields in which EO draws particles together in the plane while EHD flow, despite being short-range attractive, will repel particles at long ranges. While a Cahn–Hilliard analysis of these interactions revealed that both interactions can drive a spinodal decomposition, and will do so in a concentration-dependent manner (ESI†), the instigator of the cellular phase was not clear from this analysis alone.

To determine what interaction drove the spinodal decomposition from a film to the cellular phase, we performed a series of experiments at various φ in which V_{DC} was held constant while V_{AC} was gradually increased. First, we prepared a sample with $\varphi = 3 \times 10^{-5}$, V_{DC} = 1.9 V, and increased V_{AC} from 0.5 to 5.5 V in steps of 0.5 V. To quantify the critical AC voltage V^*_{AC} at which the cellular phase forms, the images were analyzed to count the number N of cells in each image (Fig. S10, ESI†). Fitting N *vs.* V_{AC} to a sigmoid (ESI,† eqn S16) allowed us to quantify V^*_{AC}. A typical experiment is shown in Fig. 3(a). Eight conditions were tested in triplicate (at four values of φ and both V_{DC} = 1.9 V and V_{DC} = 2.2 V) over the range of V_{AC}, enabling a Cahn–Hilliard analysis of the cellular phase formation. In this framework, spinodal decomposition is predicted to occur when the interparticle interaction (*i.e.* EO or EHD) leads perturbations to grow faster than they dissipate through diffusion (ESI†). Due to these competing effects, a general relationship is expected

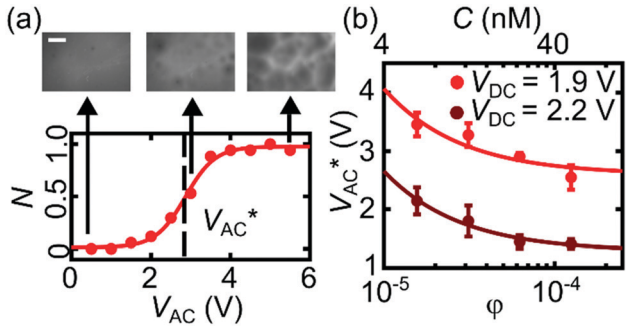

Fig. 3 (a) Using image processing, the normalized number N of cells for $\varphi = 3 \times 10^{-5}$ and V_{DC} = 1.9 V *vs.* V_{AC} are plotted and fit to a sigmoid to identify the transition voltage V^*_{AC}. Representative images displayed with a 500 μm scale bar. (b) V^*_{AC} *vs.* φ and concentration C for V_{DC} = 1.9 and 2.2 V with the lines depicting a single fit to eqn (1).

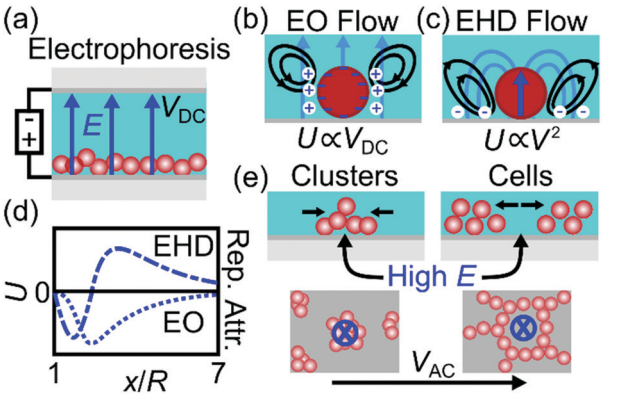

Fig. 4 Proposed mechanism of cellular phase formation. (a) With application of V_{DC}, electrophoresis moved the QDs to one electrode. (b) Once assembled into a film, electroosmotic (EO) flow produced circulating flows that promote aggregation. (c) Simultaneously, electrohydrodynamic (EHD) flow promoted aggregation at short distances, but is otherwise repulsive. (d) Flow velocity U replotted from Ristenpart *et al.*[22] *vs.* distance x from a particle of radius R for both EO (dotted line) and EHD (dashed line). (e) For small V_{AC}, EO flow dominated and particles aggregated at high field regions causing cluster formation. For larger V_{AC}, EHD dominated and produced voids at the same high field regions, nucleating the cellular phase.

wherein the strength of EHD and EO are assigned unknown, but concentration and field independent, pre-factors β_{EHD} and β_{EO}. EHD and EO scale with electric field quadratically and linearly, respectively.[22] Thus, the data in Fig. 3(b) was fit to,

$$\varphi^{-1} = \beta_{EHD}(V^*_{AC} + bV_{DC})^2 + \beta_{EO}V_{DC}, \quad (1)$$

where b reflects that while AC and DC voltages can both give rise to EHD, they may have different intensities.[22] Using nonlinear least squares fitting, we found $\beta_{EHD} = 0.004 \pm 0.001\ V^{-2}$, $b = 9.7 \pm 0.8$, and $\beta_{EO} = -0.9 \pm 0.2\ V^{-1}$. Critically, since both β_{EHD} and b were positive, this means that EHD promoted the formation of the cellular phase. In contrast, β_{EO} being negative means that EO flow inhibited the cellular phase formation. Interestingly, these results implied that V_{DC} played two competing roles by contributing to both EO and EHD. These results demonstrated that EHD flow was critical to the formation of the cellular phase.

Given that EHD was identified as an instigator, and EO an inhibitor, of the cellular phase, other features of assembly can be understood by considering where the cells form. Specifically, by performing the assembly experiment with conditions that lead to the cellular phase (V_{DC} = 2.2 V, V_{AC} = 2.0 V, $\varphi = 6 \times 10^{-5}$), leaving the field off for 40 min to allow the particles to homogenize, and then repeating the same experiment, we found that the structure of the cellular phase was repeatable with voids occurring at the same locations as shown in Fig. S11(a) (ESI†). To explore this further, an experiment was performed where a solution was exposed to conditions that led to a cellular phase (V_{DC} = 2.2 V, V_{AC} = 3.0 V, $\varphi = 6 \times 10^{-5}$), the system was then allowed to homogenize with the field off, and then exposed to conditions that led to a cluster phase (V_{DC} = 2.4 V, V_{AC} = 0 V). Importantly, Fig. S11(b) (ESI†) shows that many of the cluster phases were co-localized with the centers of the voids of the cellular phase. Together, these results suggest that features of the underlying substrate, likely asperities on the surface of the electrode, can enhance local electric field,[28] break the symmetry of the system and nucleate the phase transition. The hypothesized nucleation of the phase transformation at the regions of high field on the substrate explains the repeatable arrangement of cells that were observed when the experiment was repeated as in Fig. S11(a) (ESI†). Furthermore, the fact that the same location can lead to voids through repulsive EHD flows or clusters through attractive EO flows further suggests that the mode of spinodal decomposition is fundamentally different between EHD- and EO-mediated phases.

These experiments and analysis coalesced into a proposed mechanism for the cellular phase formation involving electrophoresis, EO flow, and EHD flow. Once V_{DC} was applied to the particle suspension, electrochemistry at the electrodes led to a DC current that electrophoretically pulled the particles to one side of the chamber as shown in Fig. 4(a). Once assembled into a film, EO led to an attractive flow that promoted particle aggregation as shown in Fig. 4(b). However, V_{AC} and V_{DC} also produced an EHD flow as depicted in Fig. 4(c) that was short-range attractive but repulsive at long ranges. Both flow profiles in Fig. 4(d) were replotted from Ristenpart *et al.*[22] Depending on which flow dominated, spinodal decomposition in Fig. 4(e) either began through an increase or decrease of particles at the high field regions, which subsequently led to the cluster phase or cellular phase, respectively. This is evident in Fig. 2(a) and 3(a) where small voids of particle-poor areas are seen initially as the cellular phase begins to form. A similar dichotomy of spinodal decompositions has been observed in simulations of colloids with competing interparticle interactions.[29,30] Interestingly, at $V_{DC} > 2.4$ V, a transition from a cellular phase to a cluster phase was observed, but this is qualitatively different than the low V_{AC} cluster phase as it occurs at the nodes of the cells. Thus, we attribute this to the vertices of the cells becoming tall enough to span the chamber, at the expense of the structure becoming thinner, at which point particles are recirculated into the voids.

With a greater understanding of the mechanism of the cellular formation, we hypothesized that the cell arrangement

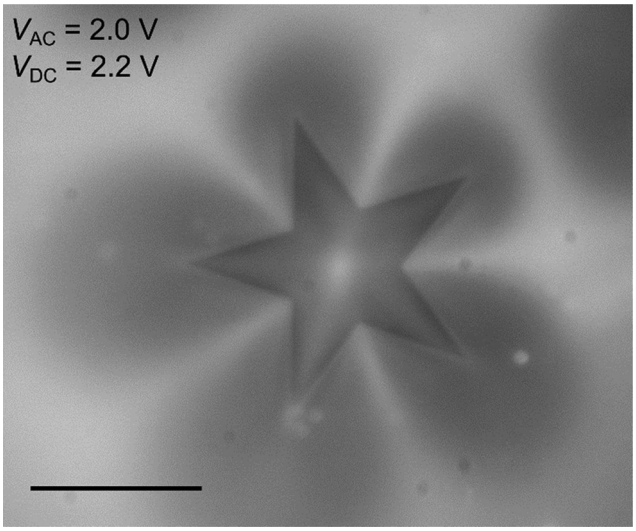

Fig. 5 Fluorescence micrograph of cells formed at the points of the star pattern where the star is the exposed ITO and the rest is covered with photoresist. Here, V_{AC} = 2.0 V, V_{DC} = 2.2 V, and $\varphi = 6 \times 10^{-5}$. The scale bar depicts 500 μm.

could be controlled. Having shown that a polymer coating prevented the formation of the cellular phase, we reasoned that photoresist could serve as a patternable coating to localize assembly. To test this, we patterned a star on the ITO slide connected to the positive lead and performed an assembly experiment. After applying V_{AC} = 2 V and V_{DC} = 2.2 V for 4 min, the cellular structure formed with cells only present centered at the points of the star (Fig. 5). Interestingly, this simple method allowed for the location and orientation of five cells to be controlled, suggesting further opportunities for crafting complex macro-porous arrangements with very low particle densities.

Considering the mechanism of formation identified in the present work and the characteristics of prior work that resulted in the cellular phase, two commonalities emerge that unify all observations of the electrically mediated cellular phase. The first commonality is that each system can be effectively reduced to 2D by way of gravity or V_{DC} pulling particles to one side of the chamber,[4,5,8] or through the formation of chains spanning the entire chamber.[6,7] The second commonality is that all feature interactions that are short-range attractive and long-range repulsive in the plane of the electrode, either through dipolar interactions of particle chains or through EHD flow. Indeed, a qualitatively similar cellular phase has been observed in suspensions of magnetic particles under the influence of triaxial magnetic fields that were effectively 2D systems in which the interaction was short-range attractive and long-range repulsive,[31–33] suggesting that these features can contribute towards a more general and complete understanding of the cellular phase.

Conclusions

We observed an ultra-low density macroscopic cellular phase through the electrically mediated assembly of nanoparticles that were an order of magnitude smaller than previous examples. Additional control experiments helped tease out the factors that contribute to cellular phase formation such as EO and EHD flows and the importance of electrochemistry at the electrode surface. This interaction between electrochemistry, electrophoresis, EO, and EHD results in a unique porous structure made of nanoparticles where the characteristic length of the pores is 10 000 times larger than the size of the particles. Importantly, by comparing to prior work, we identified two characteristics that appear to be required to form the cellular phase: particles that are confined in some way to 2D and an interparticle interaction that is short-range attractive, long-range repulsive. This level of understanding is essential to bridging the gap between observing and utilizing the unique structures produced by this assembly process.

Conflicts of interest

There are no conflicts to declare.

Acknowledgements

Acknowledgment is made to the donors of the American Chemical Society Petroleum Research Fund for partial support of this research under award 57452-DNI9. A. R. acknowledges support from the Boston University Nanotechnology Innovation Center. We acknowledge support from the Boston University Photonics Center, the College of Engineering Dean's Catalyst Award, and the Gordon and Betty Moore Foundation.

References

1 A. Füredi and R. C. Valentine, *Biochim. Biophys. Acta*, 1962, **56**, 33–42.
2 J. N. Foulc, *Adv. Mater.*, 2001, **13**, 1847–1857.
3 J. S. Park and D. Saintillan, *Phys. Rev. E: Stat., Nonlinear, Soft Matter Phys.*, 2011, **83**, 1–6.
4 M. Trau, S. Sankaran, D. A. Saville and I. A. Aksay, *Langmuir*, 1995, **11**, 4665–4672.
5 M. v. Sapozhnikov, Y. v. Tolmachev, I. S. Aranson and W. K. Kwok, *Phys. Rev. Lett.*, 2003, **90**, 4.
6 A. Kumar, B. Khusid, Z. Qiu and A. Acrivos, *Phys. Rev. Lett.*, 2005, **95**, 3–6.
7 A. K. Agarwal and A. Yethiraj, *Phys. Rev. Lett.*, 2009, **102**, 100–103.
8 S. Hardt, J. Hartmann, S. Zhao and A. Bandopadhyay, *Phys. Rev. Lett.*, 2020, **124**, 64501.
9 A. Tiribocchi, A. Montessori, M. Lauricella, F. Bonaccorso, K. A. Brown and S. Succi, *Philos. Trans. R. Soc., A*, 2021, **379**, 20200407.
10 F. Bonaccorso, A. Montessori, A. Tiribocchi, G. Amati, M. Bernaschi, M. Lauricella and S. Succi, *Comput. Phys. Commun.*, 2020, **256**, 107455.
11 A. M. Almudallal and I. Saika-Voivod, *Phys. Rev. E: Stat., Nonlinear, Soft Matter Phys.*, 2011, **84**, 1–9.

12 A. VahidMohammadi, M. Mojtabavi, N. M. Caffrey, M. Wanunu and M. Beidaghi, *Adv. Mater.*, 2019, **31**, 1–9.
13 H. Mukaibo, T. Wang, V. H. Perez-Gonzalez, J. Getpreecharsawas, J. Wurzer, B. H. Lapizco-Encinas and J. L. McGrath, *Nanotechnology*, 2018, **29**, 235704.
14 M. Chern, T. T. Nguyen, A. H. Mahler and A. M. Dennis, *Nanoscale*, 2017, **9**, 16446–16458.
15 M. Nasilowski, P. Spinicelli, G. Patriarche and B. Dubertret, *Nano Lett.*, 2015, **15**, 3953–3958.
16 W. Cao, M. Chern, A. M. Dennis and K. A. Brown, *Nano Lett.*, 2019, **19**, 5762–5768.
17 E. Bodenschatz, W. Pesch and G. Ahlers, *Annu. Rev. Fluid Mech.*, 2000, **32**, 709–778.
18 P. Bergé and M. Dubois, *Contemp. Phys.*, 1984, **25**, 535–582.
19 P. Cerisier, B. Porterie, A. Kaiss and J. Cordonnier, *Eur. Phys. J. E: Soft Matter Biol. Phys.*, 2005, **18**, 85–93.
20 H. P. Schwan, *Ann. N. Y. Acad. Sci.*, 1968, **148**, 191–209.
21 P. Ben Ishai, M. S. Talary, A. Caduff, E. Levy and Y. Feldman, *Meas. Sci. Technol.*, 2013, **24**, 102001.
22 W. D. Ristenpart, I. A. Aksay and D. A. Saville, *Langmuir*, 2007, **23**, 4071–4080.
23 S. Geiger, O. Kasian, M. Ledendecker, E. Pizzutilo, W. Fu, O. Diaz-morales, Z. Li, T. Oellers, L. Fruchter, A. Ludwig, K. J. J. Mayrhofer, M. T. M. Koper and S. Cherevko, *Nat. Catal.*, 2018, **1**, 508–515.
24 J. D. Benck, B. A. Pinaud, Y. Gorlin and T. F. Jaramillo, *PLoS One*, 2014, **9**, e107942.
25 N. A. Lewinski, H. Zhu, H. J. E. Jo, D. Pham, R. R. Kamath, C. R. Ouyang, C. D. Vulpe, V. L. Colvin and R. A. Drezek, *Environ. Sci. Technol.*, 2010, **44**, 1841–1846.
26 W. D. Ristenpart, I. A. Aksay and D. A. Saville, *J. Fluid Mech.*, 2007, **575**, 83–109.
27 A. Gencoglu, D. Olney, A. LaLonde, K. S. Koppula and B. H. Lapizco-Encinas, *J. Nanotechnol. Eng. Med.*, 2013, **4**, 1–7.
28 W. Cao and K. A. Brown, *Electrophoresis*, 2021, **42**, 635–643.
29 H. J. Zhao, V. R. Misko and F. M. Peeters, *New J. Phys.*, 2012, **14**, 063032.
30 B. A. Lindquist, S. Dutta, R. B. Jadrich, D. J. Milliron and T. M. Truskett, *Soft Matter*, 2017, **13**, 1335–1343.
31 J. E. Martin, E. Venturini, G. L. Gulley and J. Williamson, *Phys. Rev. E: Stat., Nonlinear, Soft Matter Phys.*, 2004, **69**, 1–15.
32 K. Müller, N. Osterman, D. Babič, C. N. Likos, J. Dobnikar and A. Nikoubashman, *Langmuir*, 2014, **30**, 5088–5096.
33 A. T. Pham, Y. Zhuang, P. Detwiler, J. E. S. Socolar, P. Charbonneau and B. B. Yellen, *Phys. Rev. E*, 2017, **95**, 052607.

